24th COBEM - 2017

24th ABCM International Congress of Mechanical Engineering
December 3-8, 2017, Curitiba, PR, Brazil

COBEM-2017-1884
COMPUTATIONAL ASSESSMENT OF A GAS-LIQUID PIPE SYSTEM ON THE FLUID-DYNAMICS OF A HIGH-TEMPERATURE SULFIDATION CORROSION MECHANISM

Diogo Dantas Ribeiro
Fernando Cesar Lopes de Oliveira
PETROBRAS, Petróleo Brasileiro, S.A, Rio de Janeiro, Brazil
midr@uol.com.br
fernandocesarlopes@gmail.com

Joao Coringa dos Santos Neto
PETROBRAS, Petróleo Brasileiro, S.A, Rio de Janeiro, Brazil
coringa-mec@hotmail.com

Eduardo Oliveira
PETROBRAS, Petróleo Brasileiro, S.A, Rio de Janeiro, Brazil
lusolop@gmail.com

Abstract. *Sulfidation corrosion mechanisms are strongly influenced by flow nature and distribution based on velocity fields, phases concentration and composition. On higher temperatures the vapour phase plays a major role on corrosion cracking evolution considering it's fraction of hydrogen sulfide and the conditions for wall effective collisions of sulfur components. This work focuses on the fluid dynamics of a gas-liquid flow through a computational approach regarding a carbon steel pipe system located in the feed section of an industrial fired heater. The main objective is to observe and analyze the flow characteristics that contributed to a local failure in the upstream vicinities of a tee connection mostly due to sulfidation corrosion.*
Based on a process simulation developed with Hysys® that supplied the two-phase flow characteristics and stream composition, translating an equilibrium condition, a numerical approach through CFD is structured. A block hexahedrical mesh was structured using Ansys ICEM-CFD®, being the two-phase fluid dynamics transient solution obtained with solver Ansys Fluent® through a Multi-fluid VOF and k-ω SST approach. For the accounting of Hydrogen Sulfide and Hydrogen transports on each phase, a decoupled multicomponent solution was adopted. The results showed that alterations on velocity profiles, phases volume and species fractions occurred as a consequence of flow direction changes sourced by a declined pipe transition and re-fueled by a tee reducing connection. This leaded a swirled and transitional flow on the vicinities of the failure region which established the conditions for the occurrence of sulfidation corrosion.

Keywords: *Two-phase flow, Sulfidation Corrosion, Transient Analysis, Decoupled Multicomponent Approach.*

1. INTRODUCTION

The feed pre-heating section of a hydrodesulfurization fired heater, characterized by high temperatures (above 260 ºC), hydrogen and hydrogen sulfide contents, is always susceptible to several corrosion mechanisms, which includes sulfidation, especially when the pipeline is made of carbon steel with low silicon content, below 0.10 wt% (NACE, 2014), being indifferent the content of chromium until 300 series or high alloys are used (API, 2009).

Briefly, H_2-H_2S sulfidation, similarly in terms of composition and morphology of iron sulfide scales found H2-free environments, is defined by four steps (NACE, 2014): i) scale surface adsorption of vapour sulfur; ii) sulfur compounds catalyzed decomposition and inclusion in $Fe_{1-\delta}S$ scale lattice during its nucleation and growt; iii) diffusion of cation vacancies in the $Fe_{1-\delta}S$/Fe interface; iv) interface scale forming reactions of Fe and possibly chemical transformations of sulfide film (Foroulis, 1978). Basically, it is believed (NACE, 2014), that on H_2 environments, step ii is affected. Either, hydrogen counteracts the influence of chromium (Cr) alloying additions and/or the presence of Cr has a poisoning effect

on catalytic regeneration of H_2S, thus being the reason why Cr-steel alloys are similarly resistant on this situations when compared to carbon steel (CS).

Sulfidation, represents a complex mechanism with ample room for research, for little is known about the basic mechanism of attack (Rebak, 2011). Several are its external factors, such as temperature, ranging from 230 ºC to 450 ºC, concentration and type of sulfur species, presence of naphthenic acid, velocity, local areas of turbulence, materials of construction, etc. One fact is that, given the conditions for it to establish, it will be governed by mass transport and its increases depends on the relevance of flow instabilities and regime, and local velocity aspects that can produce wall effective collisions of sulfur components.

2. WORK DELIMITATION

The study represents a case analysis of a pipe failure that characteristically suggested an occurrence of sulfidation corrosion. Objectively, this work will only focuses on fluid dynamics and mass transport aspects of the flow conditions that suggested the occurrence of sulfidation. The chemical aspects and reaction mechanisms represents a step further of the analysis done so far.

Thickness measurements and details of the interest region are shown on Fig. 1. Noticing the graphic of Fig. 1b, it is identified a circumferential uniformity of thickness loss, which is abruptly accentuated on the upstream vicinities of a branch bare 4 in "dead-leg", characterizing that local conditions established a transitional feature that possibly leaded to sulfidation. Observe (Fig. 1a) that the failure occurred between sections F and G.

Also on Fig. 1b, it is noticed that there is an increase of thickness from sections A to a maximum at section D, from which there is a continuous decrease until it reaches a minimum where the failure occurs. Notice that from this region the thickness increase until stabilizes on section L, from which remains practically constant.

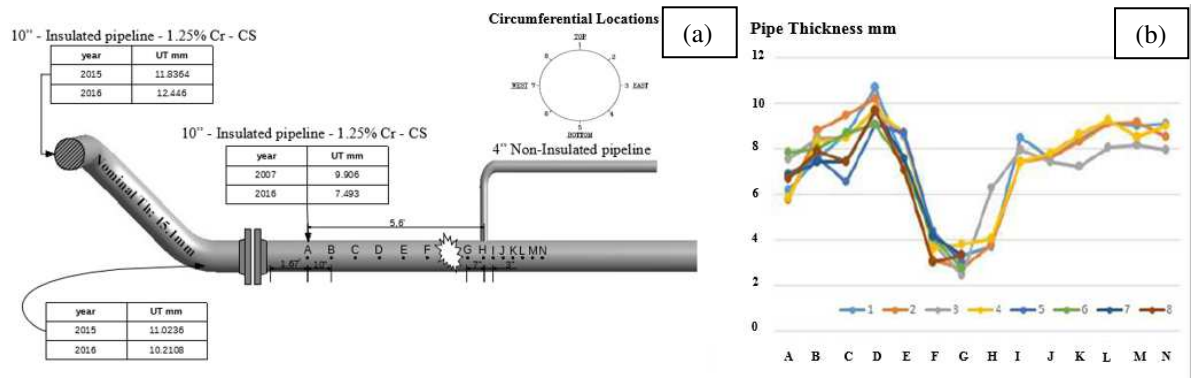

Figure 1. Thickness measurements of the 10 in pipeline. (a) Selected spots for the thickness measurements and general aspects; (b) Graphical representation of the measured thickness along the pipeline.

For the initial characterization of the flow regime, process integration simulations were done with the use of Hysys®. On them, it was observed slug flow patterns occurrences almost throughout the domain. Slug flows regimes are formed due to a further increase in vapour velocity, causing the wave at the interface to be picked up forming a frothy slug that propagates with high velocity (Collier, 1972). The Hysys® simulations revealed the transient nature of the flow, suggesting that the flow patterns observed could have create conditions for piping erosion processes. Also, it can be inferred by these results that the flow had a strong contribution on distribution of chemical species and effectiveness of its collisions over the pipe surface.

2.1 Domain Characterization, Boundary Conditions and Properties

The basis for the CFD (Computational Fluid Dynamics) through previously simulations with Hysys® based on hydrodesulfurization unit design and operating conditions.

Figure 2 shows the computational domain evaluated on this study. The fired heater feed is sent from a pre-heater through a 10 in pipe. The routing presents both vertical and horizontal segments upstream a declined pipe section with 45º degrees curves, followed by the horizontal segment where the failure occurred. The outflow to the fired heater is made with a 6 in derivation. On Fig. 2, neighboring the failure region, it is identified a non-insulated 4 in branched "dead-leg". Primarily installed for decoking processes, injecting steam and nitrogen during outages or process failure, this pipeline was blocked and out of use for a while, being removed after the failure event as a corrective measurement.

Pipelines are made of carbon steel A335 P1. Both 6 and 10 in pipe segments are insulated, being the 4 in branched pipe not insulated. The domain operating pressure is 3860 kPa with a temperature of 583.15 K.

Vapour and liquid phases reference properties are seen on Table 1, which represents the stream inlet values of Hysys® simulations, which translates an equilibrium condition for the domain. Table 2 shows the basic composition (mass and volumetric fractions) of each phase, consisting of hydrogen, hydrogen sulfide, light hydrocarbons, medium and heavy hydrocarbons, nitrogen and oxygen. On a volumetric basis, the vapour phase consists mostly of hydrogen and the liquid phase of heavy hydrocarbons.

From Fig. 2, three boundaries were defined for the simulations. The inlet boundary was prescribed as a first type BC (Boundary Condition) of mass flow normal to its surface and temperature for each phase, and a constant profile pressure of 19430 Pa in reference to the operating pressure. The liquid phase was assumed to be dispersed on the vapour phase with a volume fraction (vf) of 0.1575. A static pressure constant profile of -64045 Pa was defined for the outlet BC to the Fired Heater. The primary values adopted are resume on Table 3.

The entrance turbulence parameters were specified based on a Hydraulic Diameter (DH) of 242.8 mm and a Turbulent Intensity (IT) of 3%, for the vapour and liquid phases, estimated based on Reynolds calculated for the hydraulic diameter (Ansys, 2013). About outlet backflow considerations, the total temperature adopted was the operating temperature (583.15 K) with turbulence parameters DH and IT, respectively, of 140 mm and 2.5% for both phases.

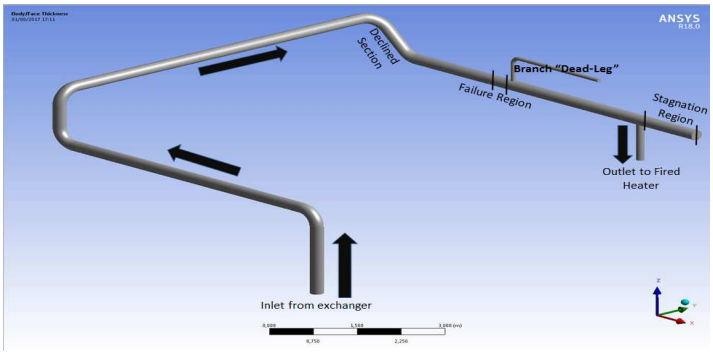

Figure 2. Tridimensional view of the computational domain pipeline.

Table 1. Reference properties adopted for each phase based on entrance streams of process simulations.

Properties	Vapour Phase	Liquid Phase
Molar Mass (kg/kmol)	24.91	205.4
Specific Mass (kg/m3)	19.86	595.3
Specific Heat (kJ/kg.ºC)	3384	2971
Thermal Conductivity (W/m.K)	0.1677	0.07779
Viscosity (cP)	0.0282	0.1354

Table 2. Inlet profile of phases composition (Mass and Volumetric Fractions)

Components	Vapour Phase		Liquid Phase	
	Mass Fraction	Mole Fraction	Mass Fraction	Mole Fraction
Hydrogen	0.062715	0.774824	0.000595	0.060574
Hydrogen Sulfide	0.016629	0.0125154	0.000484	0.002915
Nitrogen	0.003413	0.003	0.000035	0.000274
Oxygen	0.000149	0.0001	0.000002	0.000014
Light Hydrocarbons	0.098288	0.1009656	0.002514	0.017979
Medium and Heavy Hydrocarbons	0.818806	0.108595	0.99637	0.918244

Table 3. Boundary Conditions - Reference Values

BC Variable	Inlet		Outlet	
	Vapour	Liquid	Vapour	Liquid
Mass Flow (kg/s)	8.57	13.21	-	-
H2S Mass Fraction	0.016628	0.000484	0.016615	0.000482
H2 Mass Fraction	0.062715	0.000595	0.062656	0.000592

An estimation of the system pressure loss was made based on pipes effective lengths (l_{ef}), pressure difference calculated with Hysys® (0,36092%) and approximations considering Darcy-Weisbach equation with the addition of specific heat loss (Q W/m^3) and level difference (z m), as shown on Eq. (1). On this, the friction factor (f) was calculated with Colebrook Formulation (Colebrook, 1939), ρ_m represents the mixture density of the gas-liquid flow (47,03 kg/m^3), D_{in} the internal diameter (m) of each pipe segment considered, w the mixture mass flow (kg/s) and γ the specific weight (N/m^3). Using a weighting average approach between all obtained values, a reasonable pressure loss resulted to be 2,15%. Additionally, for the heat losses estimative, adopting an iterative thermal resistance methodology, calculations were made based on ABNT, 2012, ISO, 2008, Incropera, *et al.*, 2016 and Petrobras, 2012, with the properties and values presented on Table 4, assuming a wind speed of 5 m/s (Meteoblue, 2016) and an ambient temperature of 20 ºC.

$$\Delta p = \left(\frac{1{,}18993 \cdot 10^{-4} \cdot f \cdot l_{ef} \cdot w^2}{\rho_m \cdot d_{in}{}^5} \right) + \frac{Q \cdot w}{\rho_m} + z \cdot \gamma \tag{1}$$

Table 4. Properties and parameters used for the thermal calculations and pressure loss estimation

Thermal and Dynamic Properties, and General Parameters	Pipe Segment		
	4 in[(1)]	6 in	10 in
Effective Length m	2.68	21.25	33.01
Thickness mm	11.125	14.275	15.088
Heat Transfer Coefficient W/m^2.K	13.5	17.2	20.84
Radiation Heat Transfer Coefficient W/m^2.K	0.973	0.944	19.98
Friction Factor	-[(2)]	0.0287	0.03395
Insulation Materials	Carbon Steel	Aluminum	Calcium-Silicate
Thickness mm	-	0.6096	50.8
Thermal Conductivity W/m.K	48	237	0.081
Emissivity	0.96	0.15	-
Specific Heat J/kg.K	458.5	871	1030
Density kg/m^3	7865	2719	245

[(1)] the 4 in "dead-leg" was defined as non-insulated, as identified on the happening of the failure event
[(2)] a stagnated flow was assumed for the 4 in "dead-leg", on which only in the interface region near zero velocities would developed depending on the extension of recirculation zones

Based on Table 4, all walls were modelled using a mixed third type wall boundary condition with a shell conduction model (Ansys, 2013), being all pipelines, but the 4 in "dead-leg", insulated. This was done considering a sensibility steady analysis comparing test cases with imposed heat flux (second type) and third type BC. As shown on Fig. 3, the third type was the one that better captured the physical behavior expected. On Fig. 3a it is seen that despite being insulated, the 4 in pipe, as a region of stagnated flow, tends to develop an equilibrium state diffusing the temperature to its end, which could have influenced the adjacencies between 4 and 10 in pipes. As expected, with a non-insulated 4 in pipe (Fig. 3b), a more pronounced temperature transition is observed, but still with the temperature being diffused throughout the pipe. Otherwise, Fig. 3c shows that with a 3rd type BC the diffusion is less propagated and a well-defined thermal entrance length is observed on both phases.

Regarding the domain characterization, a block hexaedrical prism mesh was structured with Ansys ICEM-CFD® consisting of 1,3 M elements divided in 4 M faces and 1,3 M nodes. Figure 4 shows details of the mesh developed. Three regions of interest are shown, the connection between 4 and 10 in pipes, the declined pipe upstream from the failure region and the outlet to Fired Heater. Prism mesh elements and higher grid resolutions were implemented based on two objectives regarding near-wall region (inner layer), first to capture through basically wall functions the viscous sublayer and buffer-layer on the adjacencies of the 10-4 connection, and second to capture boundary layer effects (log-law layer), approximately solving buffer-layer aspects, on this and the outlet region. On this matter, based on Ansys 2013, Durbin, 1991, Launder and Spalding, 1974 and Salim and Cheah, 2009, the y+ was regulated below 15 on the pipe connection, and between 20 and 60 on the failure region and adjacencies of the outlet, as observed on Fig. 5 mostly for both phases. Notice that for the liquid phase on these regions, due to the higher velocities developed and flow acceleration, the y+ is higher, but still was sufficiently below 300 on transitions, entrance length and adjacencies of the tee reducing connections, well capturing the development of the velocity profile on both.

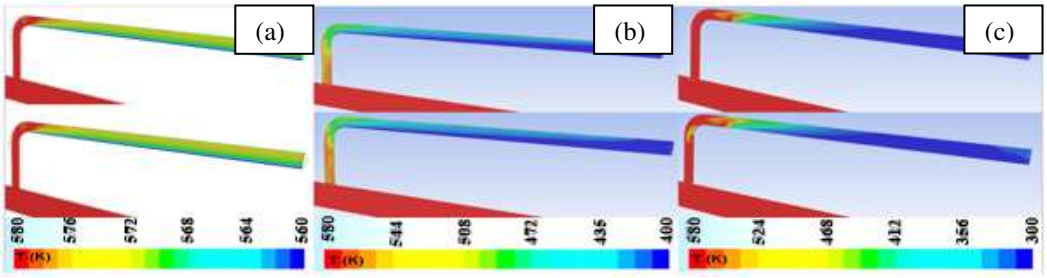

Figure 3. Axial plane plots colored by temperature focusing the 4 in pipe and connection. Above: vapour phase results; Below: liquid phase results. (a) Pipes walls insulated with 2nd type BC; (b) Non-insulated 4 in pipe with 2nd type BC; (c) Non-insulated 4 in pipe with 3rd type BC.

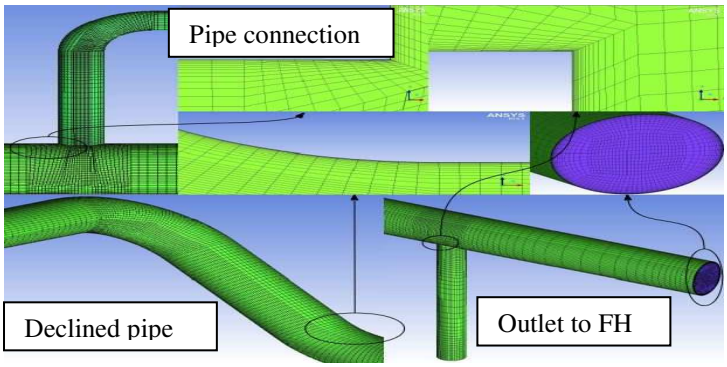

Figure 4. Mesh details focusing prism layers and higher resolutions grids.

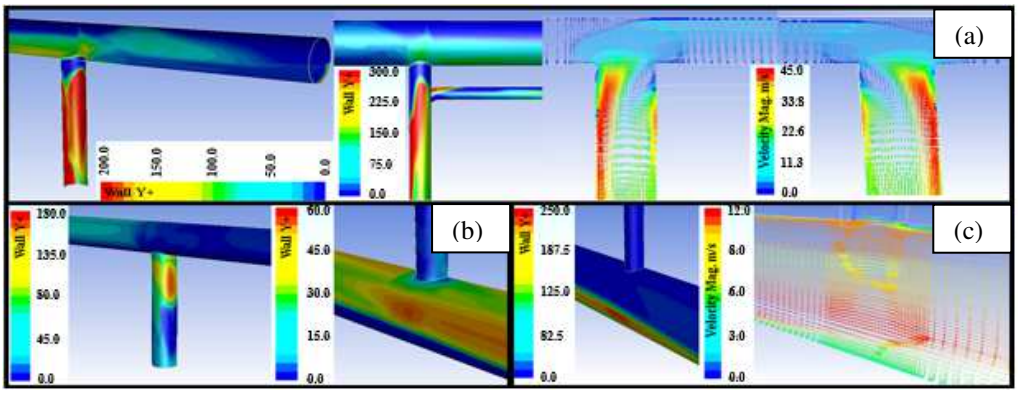

Figure 5. Mesh resolution regarding the y+ and velocity profiles (vectors colored by velocity magnitude) obtained for the converged steady simulation with 3rd type BC. (a) Tee reducing connection 10-6 in and stagnation regions results for liquid phase; (b) Tee reducing connections 10-4 and 10-6 in results for vapour phase; (c) Tee reducing connection 10-4 in results for liquid phase.

2.2 Mathematical Models and Computational Procedures

As a first approximation, each phase was considered as a pseudo-component, whose pseudo-properties are obtained through volumetric fraction weighting based on composition given by Hysys® solution response. On flow temperature and pressure range, it was identified gaseous species compounding the liquid phase and liquid species, the vapour phase. Comparison of each component saturation temperature with flow temperature gross variation (between 305 and 310 ºC), revealed that no phase changes is expected for the simulation conditions analyzed. Therefore, this implicates that the migration of species could only happen through diffusion, what permits to assume a multiphase multicomponent approach that includes both specie transfer between phases and its transport through each phase bulk.

The physical meaning of the precedent identifications was in case of considering one phase dispersed or dissolved into the other, therefore denoting the flow transitional nature or its dynamic instability. On this subject a way to model the problem was defining the liquid phase as dispersed on the vapour phase, which could be done through an eulerian approach, where each phase comprise separated continuum, however interpenetrated.

Supposing interaction of specie-mass transfer between phases, this would require a coupled solution for the species transport, therefore resulting in a high computational cost with foreseen difficulties regarding its stability and convergence. Initial tests showed exactly this, and being the diffusion a secondary effect in terms of the flow development, a more reasonable approach would be to solve the species transport in a decouple manner, neglecting the interaction between phases. Moreover, the heat (Pe_h) and mass transfer (Pe_sp) Péclet numbers for each phases resulted: Pe_h = $9.06.10^{-5}$ and Pe_sp = 5.10^{4} - vapour phase; Pe_h = $2.64.10^{6}$ and Pe_sp = $2{,}56.10^{3}$ - liquid phase, which in all cases are values >> 1, reflecting an advection-dominant problem (Wesseling, 2001 and Kirby, 2010).

On this sense, diffusion was considered relevant in relation to corrosion chemical action as a result from the flow characterization in terms of recirculation zones, secondary vortex formations and two-phase regime, therefore the strategy of a decoupled solution through only the aspects of species transport.

The solver Ansys Fluent® was used in order to solve the two-phase fluid dynamics and species transport on steady and unsteady regimes . Based on the precedent discussion, this was done considering the embedding of sharpening schemes through the eulerian Multi-fluid VOF (Volume of Fluid) approach with a damping source term, regulated at 100, added for correction of turbulence quantities treated with the *k-ω* SST (Shear Stress Transport) model. The choice of this model was a result from initial attempts with k-ε Realizable two-layer approach. Non-physical disturbances were observed on all cases tested that resulted eventually on solution divergence. Given the mesh resolution, *k-ω* SST has the advantage of being relatively y+-insensitive (Ansys, 2013) and can dealt better with interface turbulence generation due to velocity gradients and instabilities through a source term with damping factor added to the ω-equation.

Regarding the multiphase interface solution strategy:

i) interfacial area concentration treated with a symmetric model;
ii) momentum coefficient exchanges obtained through Schiller and Naumann, 1935 model with drag modification by the Brucato, *et al.*, 1998 correlation (increases the drag coefficient by turbulence from the liquid phase);
iii) turbulent dispersion (accounts the turbulent momentum transfer between phases through additional dispersion from turbulent fluctuations) modelled with Simonin and Viollet, 1990 model;
iv) surface tension assumed as constant (0.006609 N/m from Hysys® entrance boundary) and modelled with the Continuum Surface Force model (Brackbill, et al., 1992), which represens the recommendation (Ansys, 2013) for this scenario.

The estimative of the dispersed phase particle diameter was done through different approaches for gas-liquid flows (volume median diameter by Tatterson, *et al.*, 1977 (d_{vm} = $3.79.10^{-4}$ m) and Kataoka, *et al.*, 1983 (d_{v50} = $5.71.10^{-4}$ m), and sauter mean diameter ($d_{32}^{0.65}$ = $1.12.10^{-3}$ m and $d_{32}^{1.3}$ = $1.12.10^{-3}$ m) and maximum diameter (d_{max} = $4.495.10^{-3}$ m) by Fore, *et al.*, 2002 and Kocamustafaogullari, *et al.*, 1994). Linearizing these values, was seen that a reasonable estimation, based on the limitations and scope of each model, was 1.12 mm, almost equal to the d_{32} value with a coefficient of 0.65.

The vapour phase pseudo-component density was treated with a Real Gas Peng-Robinson model regarding the majority presence of hydrogen among several hydrocarbons, allowing the capture of its compressibility. Therefore, its pseudo-properties were implemented through volumetric fraction average weighting resulting the following calculated values: Acentric Factor = -0.030496; Critical Pressure = 1.8411 MPa; Critical Temperature = 130.41 K; and Critical Volume = 0.020799 m^3/kg. Whereas, the liquid phase density was established as constant with a value of 595.3 kg/m^3.

The decoupled analysis, on steady and unsteady states, of species transportation was made through the embedding of mixture templates considering three species on each phase. On this sense, two mixture templates was formulated, each with a pseudo-component that represent the bulk phase and two chemical species (H_2 and H_2S).

The steady state analysis were developed using a pseudo-transient approach initialized with a hybrid solution (potential flow). This method represents an implicit under-relaxation which controls a fictitious time on fluid time scale, being a way to increase and regulate the stability of stationary problems. The pseudo-time step was regulated as 0.001 s, which served as base for the transient analysis time step.

To establish a reasonable mean residence time for the transient calculations, a RTD (Residence Time Distribution) method was evaluated based on Li and Cheng, 2010 using the step method. On this case, two tracers are defined as a continuum embedded with mixture templates for the solution of each tracer specie transport equation. Using a steady converged solution (based on the steady cases solved) and a user-defined scalar (passive tracer), the results are store and then applied for the solution of Eq. (2), where C_{max} is the maximum volumetric concentration on the integral interval and t_{mean} the mean residence time. The estimative resulted a t_{mean} of 4.58 s and 2.36 s, for the liquid and vapour phases, respectively. This required that aiming robust results, the transient simulations should be analyzed only after 9 s of total time simulation on a range of at least 14 s, what implicates the cover of three (liquid phase) and five (vapour phase) residence times.

$$t_{mean} = \frac{1}{\Delta C} \int_{C'}^{C_{max}} t dC \tag{2}$$

The transient solution was structured based on these RTD results and with an initialization from a steady converged simulation with 3rd type BC, regarding wall heat transfer. Then, given the transient fields obtained for the two pseudo-component and two phase flow, a decoupled multicomponent solution was developed accounting the transport of hydrogen sulfide and hydrogen of each phase. In order to obtain stable results for the unsteady cases, the solution behavior was monitored adjusting the time steps on a range between 0.001 s and 0.005 s, being the time variable discretized with a 1st order implicit scheme.

The numerical method used was a pressure based pressure-velocity coupling implicitly coupled due to the continuous phase being compressible. Problem variables were treated with 3rd order interpolation schemes (QUICK and MUSCL), therefore avoiding numerical diffusion on regions with poor and coarser mesh resolutions. Turbulence quantities were treated with 1st order upwind scheme, due to numerical instabilities and oscillations. Stability and convergence of the solution, especially on steady state, were monitored through Nusselt ratio between Dittus-Boelter correlation and effective value, Pressure Loss, Volumetric Fraction (VF) and Velocities on sections located adjacent to the tee 10-4 and 10-6 connections, and outlet.

3. RESULTS AND DISCUSSION

3.1 Steady Multiphase Analaysis

As observed on Fig. 6, it is seen that the steady solution showed that the flow is characterized by a transitional nature downstream the declined pipe until the 10-4 in connection. Jet occurrence disturbed by swirl formations are especially seen immediately downstream the declined pipe (Fig. 6c). Basically, the dispersed liquid jet in a froth form could alter the phase distributions, therefore dislocating the vapour phase along pipeline and so altering the circumferential concentration of hydrogen sulfide, as seen on Fig. 6d.

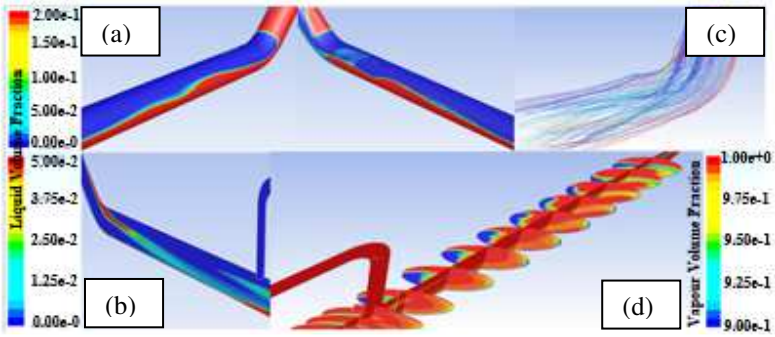

Figure 6. VF distributions on the proximities of the failure region (steady simulation). (a) Wall liquid VF; (b) Longitudinal section liquid VF; (c) Stream lines colored by liquid VF identifying swirl instabilities downstream the declined pipe; (d) Longitudinal and Cross-sections of vapour vf.

Figure 7b shows that the declined pipe drove the flow towards the east (refer to Fig. 1) which lead it to spread on the east surface from bottom-west. Notice that this path is complemented on the z direction (Fig. 7a), for the flow is drove towards top from the east and west, descending from the top-east. Merging these paths, on the failure region (F and G sections) stagnations are expected between top-east and bottom-west, both locations where most collisions occurred, as it can be seen on Fig. 7c and d, mostly regarding vapour H2S mass fraction. This characterization is important, because when focusing on a possible sulfidation mechanism, the vapour phase effective collisions will govern the way failure would happen. This is reinforced by the graphics of Fig. 8a, b and c. It reveal that neither erosion nor wall shear stress from the liquid phase could be a lead actor for the pipe system failure. Figure 8a shows that the estimative of wall shear stress are negligible for the vapour phase, as expected, and regarding the liquid phase are higher on the east and bottom-west positions, presenting a transition peak in location 3 immediately downstream from flange and a disruption in location 6 (failure region). But, still the values are below 100 Pa, being in the range observe typically on two phase flow regimes, especially in slug flow occurrence. According to Kahyarian *et al.*, 2017, the values identified here are unlikely to suggest a mechanical removal of protective films or layers by mechanical forces. However, based on Farrell and Roberts, 2010, once formed the $Fe_{1-\delta}S$ scale, being this a weak crystal lattice subject to wear, the values observed could be sufficient for its removal and advance of sulfidation mechanism.

Figure 8c shows that erosional velocities, based on API, 1991, are much higher then the maximum velocities estimated on both phases in all sections observed. The values calculated refer to Eq. (3), where V_e is the fluid erosional velocity, ρ_m the mixture density and c a empirical constant assumed as 100 (continuous services virtually free of solids). For a matter of being conservative, three different approaches are used for ρ_m estimation, Eqs. (4), (5) and (6), where Sl and S_g, liquid (water = 1) and vapour (air = 1) specific gravity on standard conditions, R_{gl} the vapour/liquid ratio, P_{act}

and T_{act} the operating pressure and temperature, Z the compressibility factor, G_g and G_l, the vapour and liquid mass velocities, ρ_g and ρ_l, the vapour and liquid densities, and α the volumetric fraction, being all unities expressed in SI.

$$V_e = \frac{0.0348 \cdot c}{\sqrt{16.02 \cdot \rho_m}} \tag{3}$$

$$\rho_m = \frac{1800 \cdot S_l \cdot P_{act} + 0.3916 \cdot R_{gl} \cdot S_g \cdot P_{act}}{28.82 \cdot P_{act} + 1.8 R_{gl} \cdot T_{act} \cdot Z} \tag{4}$$

$$\rho_{ave} = \frac{G_g + G_l}{(G_g / \rho_g) + (G_l / \rho_l)} \tag{5}$$

$$\rho_m = \alpha \cdot \rho_v + (1 - \alpha) \cdot \rho_l \tag{6}$$

Still on Fig. 8c, it is observed the swirl number (SN) for the two phases, calculated according Eq. (7), where G_θ is the axial flux of angular momentum and G_a the axial flux of axial momentum, and D_{ref} is the pipe internal diameter. Referring to Ansys, 2013, values of SN higher than 0.5 are characterized as highly swirling flows, which is observed rightly downstream of the declined section, reinforcing what was mentioned on Fig. 6c. Besides, it is clearly observed that upstream from failure region the SN begins to increase, characterizing that both the declined pipe transition and pipe tee reduction 10-4 in have contributed on supplying turbulence energy that increased the flow disturbance on this regions, affecting the diffusion and collisions of chemical species, specially H_2S.

$$SN = \frac{2 \cdot G_\theta}{D_{ref} \cdot G_a} \tag{7}$$

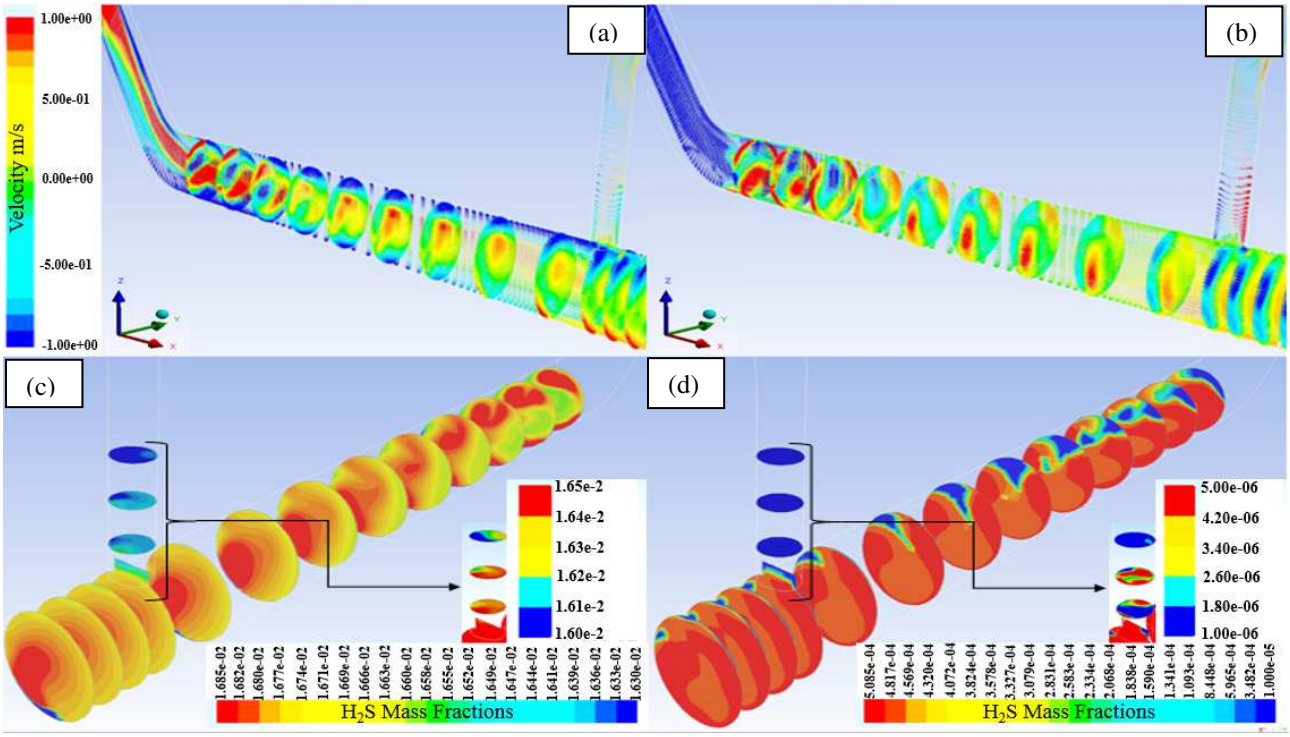

Figure 7. Vector plots colored by velocities and profiles of Vapour phase. (a) Z-Velocity m/s; (b) Y-Velocity m/s; (c) Vapour Phase mass fraction of H_2S; (d) Liquid Phase mass fraction of H_2S.

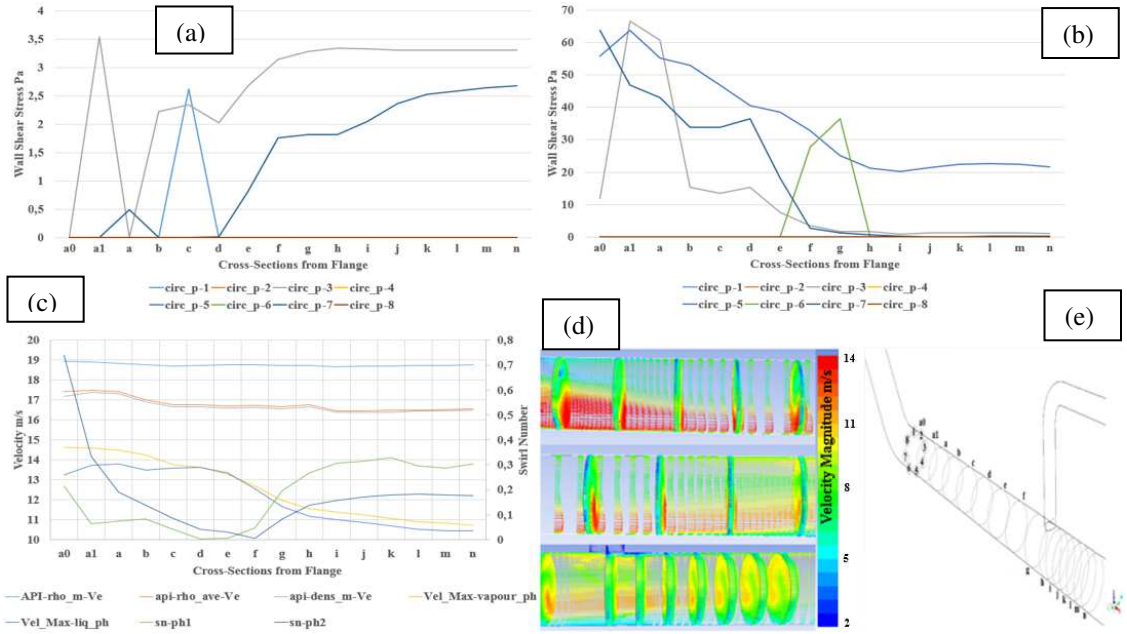

Figure 8.Stedy results: (a) Wall Shear Stress of Vapour phase; (b) Wall Shear Stress of Liquid Phase; (c) Erosional Velocities, Maximum Velocities and Swirl number for vapour (ph1) and liquid (ph2) phases; (d) Velocity Profiles colored by Magnitude m/s for Vapour phase; (e) Cross-Sections and Circumferential Points (circl_p) position.

3.2 Unsteady Multiphase Analaysis

Figures 9 and 10 shows the results obtained with the unsteady simulation. On Figs. 9a and b, it is noticed that through time intense recirculations and vortexes are formed, similarly to what was described for the steady simulation, characterizing the transitional nature of the flow and its swirling aspects downstream from the declined pipe and when approaching the tee connection. Most important are the aspects observed on Fig. 9c, that clearly define a slug flow regime. Notice that on interval 11 to 14 s, a wave is lifted from the declined pipe forming a frothy that propagates throughout failure region towards the tee connection.

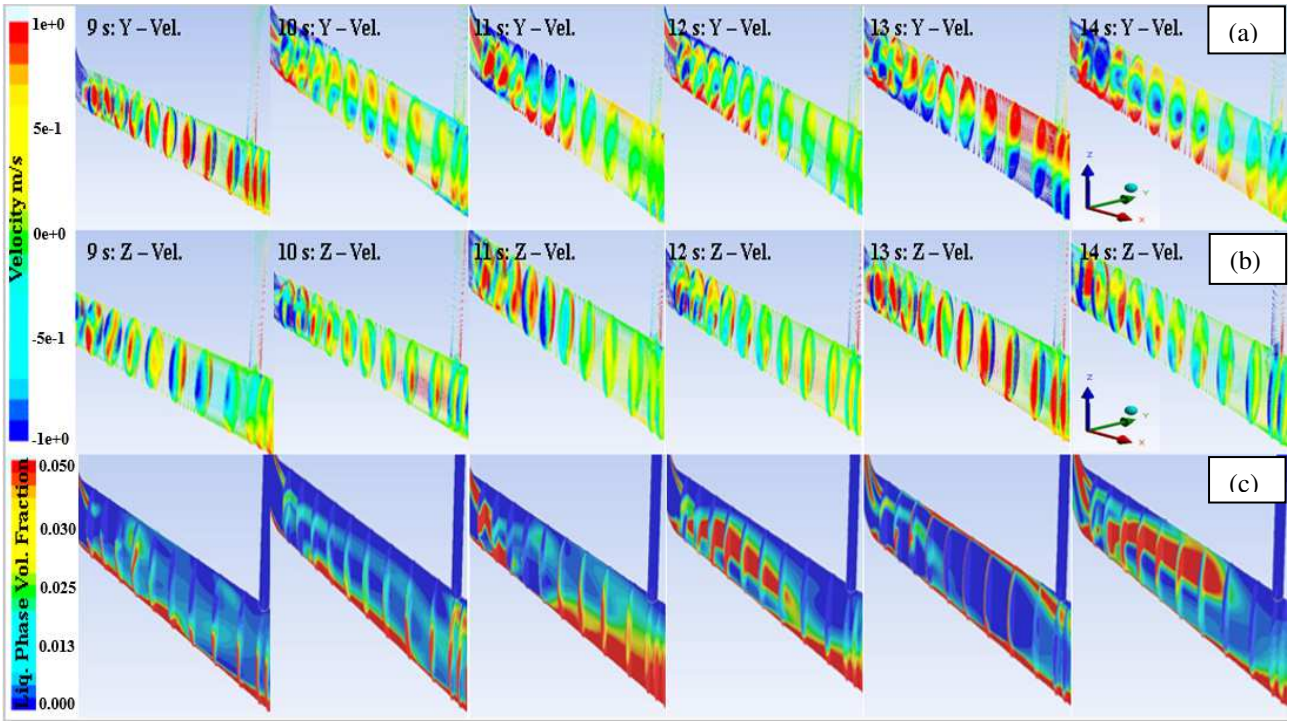

Figure 9. Flow distribution upstream the failure region in terms of simulation time: (a) Velocity vectors colored by y velocity (vapour), (b) Velocity vectors colored by z-velocity (vapour); (c) Liquid phase volumetric fraction.

Comparing Figs. 9 and 10, the mass fraction H_2S distribution coincides to what is expected based on slug and turbulent nature of the flow. This indicates that most likely collisions were effective on top-east and bottom-west reflecting the flow swirling aspects. Most important, the interrelation between flow and species transportation that was identified on these results suggests that a presumed probably density function in conjunction with look-up tables can be used to estimate the free energy variations from species collision and roughly predict the expected rate of sulfidation corrosion.

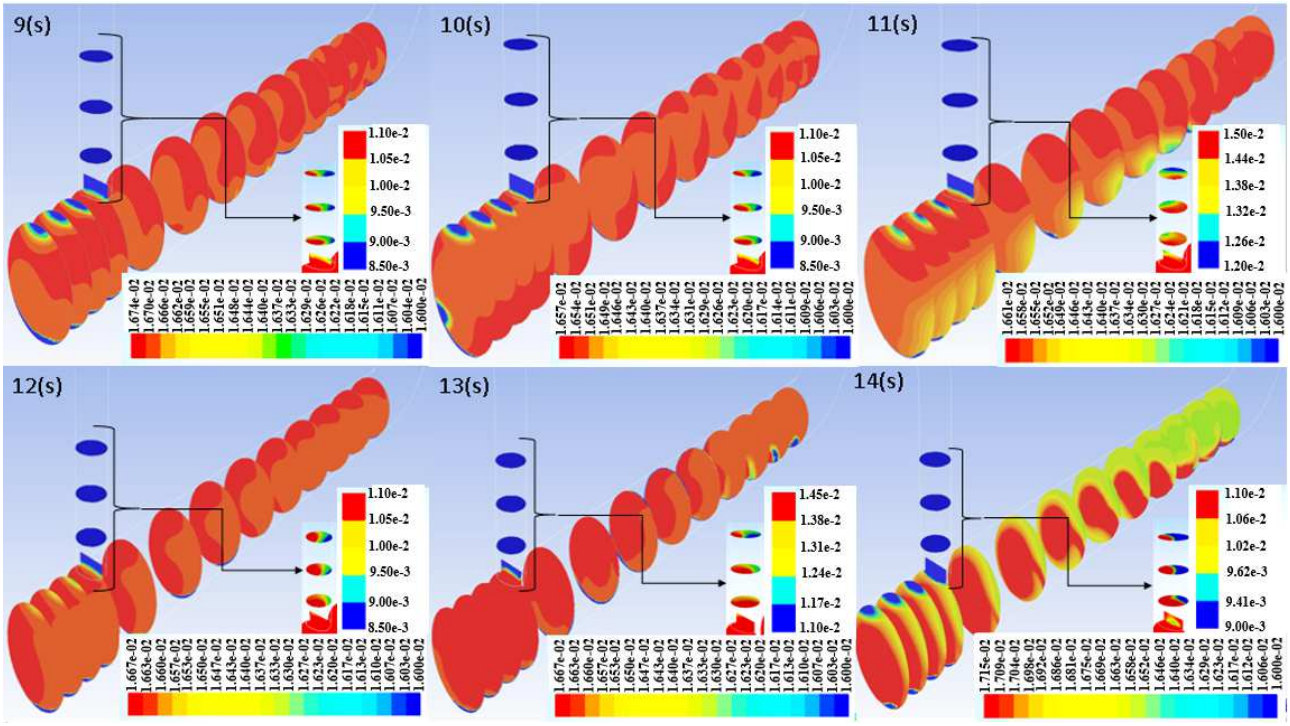

Figure 10.Vapour phase mass fraction of H_2S across simulation times.

4. CONCLUSIONS

Changes on velocity profiles and volume fractions occurred on the failure region mainly due to the declined pipeline in a 45º curve, being this re-fueled from a secondary turbulence source on vicinities of tee reducing 10-4 in connection. Unsolved instabilities were clearly seen as a froth transitional nature of the flow observed on the interest region, clearly identifying a slug flow pattern, based on unsteady results. The liquid phase projection from the declined pipe uplifted and reinforced on approximation to the tee connection, clearly had a severe impact on terms of chemical species collisions, denoting probably a sulfidation mechanism, explaining the uniform circumferential material wear but with increased intensity changes along the pipeline.

Based on the aspects mentioned and adding the effect of the stagnation zone created by the branched “dead-leg”, which increased the concentration of vapour sulfur species on the failure region, the chemical aspect was truly the distinctive action that resulted on an increase of thickness loss on the upper generating line of the main 10 in pipeline upstream the branch connection.

Further investigation are required regarding the interrelation between flow and species transportation on high temperature sulfidation. A possibility that can be test, analogously to what is done on combustion models such as steady diffusion flamelet, is the use of a presumed probably density function in conjunction with look-up tables to estimate the free energy variations from species collision and roughly predict the expected rate of sulfidation corrosion.

5. REFERENCES

ABNT NBR, 2012. *10662 - Isolantes térmicos pré-moldados de silicato de cálcio - Especificação*. ABNT, Rio de Janeiro, 2nd Edition.

API, 1991. *Recommended Practice for Design and Installation of Offshore. Production Platform Piping Systems: API RECOMMENDED PRACTICE 14E (RP 14E)*. API, Washington, 5th Edition.

API, 2009. *Guidelines for Avoiding Sulfidation (Sulfidic) Corrosion in Oil Refineries: API RECOMMENDED PRACTICE 939-C*. API, Washington, 1st Edition.

Ansys, 2013. *Fluent Manual: Theory Guide 15.0*. ANSYS, Inc., USA.

Brackbill, J. U., Kothe, D. B., and Zemach, C., 1992. "A Continuum Method for Modeling Surface Tension". *J. Comput. Phys*. Vol. 100, pp. 335 – 354.

Brucato, A., Grisafi, F., and Montante, G., 1998. "Particle drag coefficients in turbulent fluids". *Chemical Engineering Science.*, Vol. 53 (18), pp. 3295 – 3314.

Colebrook, C. F., 1939. "Turbulent flow in pipes with particular reference to the transition region between the smooth and rough pipe laws". *J. Instituion of Civil Engineers*., Vol. 11, No. 4, pp. 133 – 156.

Collier, J. G., 1972. *Convective Boiling and Condensation*. McGraw-Hill, London, 1st edition.

Durbin, P. A., 1991. "Near-Wall Turbulence Closure Modelling Without "Damping-Functions"". *Theoret. Comput. Fluid Dynamics.*, Vol. 3, pp. 1 – 13.

Farrell, D., and Roberts, L., 2010. A study of high temperature sulfidation under actual process conditions. In *Proceedings of the NACE Internation Corrosion 2010 Conference & Expo*. Texas, USA.

Fore, L. B., Ibrahim, B. B. and Beus, S. G., 2002. "Visual Measurements of droplet size in gas liquid annular flow". *Int. J. Multiphase Flow.*, Vol. 28, pp. 1895 - 1910.

Foroulis, Z. A., 1978. "Kinetics and mechanism of the reaction of iron with sulfur vapor in the temperature range of 250 to 500ºc". *Werkstoffe and Korrosion*, Vol. 29, pp. 385 - 393.

Incropera, F. P., DeWitt, D. P., Bergman T. L., and Adrienne S. L., 2016. *Fundamentals of Heat and Mass Transfer*. John Wiley & Sons, Hoboken, 6th Edition.

ISO, 2008. *12241 - Thermal insulation for building equipment and industrial installations - Calculation rules*. ISO, Geneva, 2nd Edition.

Kirby, B. J., 2010. *Micro- and Nanoscale Fluid Mechanics*. Cambrigdge University Press, New York, 1st Edition.

Kahyarian, A., Achour, M., and Nesic, S., 2017. *CO2 corrosion of mild steel. In: Trends in Oil and Gas Corrosion Research and Technologies - Production and Transmission.* Elsevier, Massachusetts, Ch. 7, pp. 149 – 182.

Kataoka, I., Ishii, M., and Mishima, K., 1983. "Generation and size distribution of droplet in annular two-phase flow". *J. Fluids Sci.* Vol. 105, pp. 230 – 238.

Kocamustafaogullari, G., Smits, S. R. and Razi, J., 1994. "Maximum and mean droplet sizes in annular two-phase flow". *Int. J. Heat Mass Transfer*. Vol. 37, pp. 955 – 965.

Launder, B. E., and Spalding, D. B., 1974. "The Numerical Computation of Turbulent Flows". *Comp. Meth. In App. Mech. And Engineering*. Vol. 3, pp. 269 – 289.

Li, G., and Cheng, C-Y., 2010., "Various approaches to compute fluid residence time in mixing systems". In *Proceedings of the ASME 2010 3rd Joint US-European Fluids Engineering Summer Meeting and 8th International Conference on Nanochannels, Microchannels, and Minichannels – FEDSM-ICNMM2010-30771*. Montreal, Canada.

Meteoblue, 2016. "Weather – Close to you". 5 Nov. 2016 < https://www.meteoblue.com/pt/tempo/previsao/archive/>.

NACE International, 2014. Item no. 24222 - Overview of Sulfidation (Sulfidic) Corrosion in Petroleum Refining Hydroprocessing Units. NACE International Publication, Houston, 2014 Edition.

Petrobras, 2012. *N-0894 - Projeto de Isolamento Térmico a Baixa Temperatura*. CONTEC, Rio de Janeiro, 5th Revision.

Rebak, R. B., 2011. "Sulfidic corrosion in refineries - a review". *Corros. Rev.*, Vol. 29, pp. 123 - 133.

Salim, M. S., and Cheah, S. C., 2009. "Wall y+ Strategy for Dealing with Wall-bounded Turbulent Flows". In: *Proceedings of the International Multiconference of Engineers and Comp. Sciences – IMECS2009.* Vol. II. Hong Kong.

Simonin, O., and Viollet, P. L., 1990. "Modelling of Turbulent Two-Phase Jets Loaded with Discrete Particles". *Phenomena in Multiphase Flows*., pp. 259 – 269.

Schiller, L., and Naumann, Z., 1935. "A drag coefficient correlation". *Z. Ver. Deutch. Ing*. Vol. 77, pp. 318 – 320.

Tatterson, D. F., Dallman, J. C., and Hanratty, T. J., 1977. "Drop sizes in annular gas-liquid flows". *American Institute of Chemical Engineers Journal*. Vol. 23 (1), pp. 68 - 76.

Wesseling, P., 2001. *Principles of Computational Fluid Dynamics*. Springer-Verlag, Berlin.

6. RESPONSIBILITY NOTICE

The authors are the only responsible for the printed material included in this paper.